To appear AIAA J.

Evaluation of turbulence-model performance in jet flows

S. L. Woodruff
Department of Mathematics and School of Computational Science and Information Technology,
Florida State University, Tallahassee FL 32306-4120

J. M. Seiner
National Center for Physical Acoustics,
University of Mississippi, University, MS 38677

M. Y. Hussaini
School of Computational Science and Information Technology,
Florida State University, Tallahassee FL 32306-4120

G. Erlebacher
Department of Mathematics and School of Computational Science and Information Technology,
Florida State University, Tallahassee FL 32306-4120

Introduction

The importance of reducing jet noise in both commercial and military aircraft applications has made jet acoustics a significant area of research [1]. A technique for jet noise prediction commonly employed in practice is the MGB approach [2], based on the Lighthill acoustic analogy [3]. This technique requires as aerodynamic input mean flow quantities and turbulence quantities like the kinetic energy and the dissipation. The purpose of the present paper is to assess existing capabilities for predicting these aerodynamic inputs. Two modern Navier-Stokes flow solvers, coupled with several modern turbulence models, are evaluated by comparison with experiment for their ability to predict mean flow properties in a supersonic jet plume. Potential weaknesses are identified for further investigation. Another comparison with similar intent is discussed by Barber *et al.* [4]. The ultimate goal of this research is to develop a reliable flow solver applicable to the low-noise, propulsion-efficient, nozzle exhaust systems being developed in NASA focused programs. These programs address a broad range of complex nozzle geometries operating in high temperature, compressible, flows.

Seiner *et al.* [5] previously discussed the jet configuration examined here. This convergent-divergent nozzle with an exit diameter of 3.6 in. was designed for an exhaust Mach number of 2.0 and a total temperature of 1680° F. The acoustic and aerodynamic data reported by Seiner *et al.* [5] covered a range of jet total temperatures from 104° F to 2200° F at the fully-expanded

nozzle pressure ratio. The aerodynamic data included centerline mean velocity and total temperature profiles.

Computations were performed independently with two CFD codes, ISAAC [6] and PAB3D [7]. Turbulence models employed include the $k-\varepsilon$ model [8], the Gatski-Speziale algebraic-stress model [9] and the Girimaji model [10], with and without the Sarkar compressibility correction [11]. Centerline values of mean velocity and mean temperature are compared with experimental data.

Codes and Models

ISAAC (Integrated Solution Algorithm for Arbitrary Configurations) [6] is a finite-volume code of second-order accuracy which solves the full Favre-averaged Navier-Stokes equations. An upwind scheme based on Roe's flux-splitting is used for the convective terms, central differencing for the diffusion terms and an implicit, spatially split, approximate-factorization scheme for iteration.

The PAB3D code [7] solves the Reynolds-averaged Navier-Stokes equations in a thin-shear-layer approximation. Diffusion terms are central-differenced. The implicit iteration operator employs the van Leer scheme and the explicit terms (*e.g.*, convective terms) are evaluated with the Roe scheme.

The grid used here is composed of five blocks, one in the nozzle (61×61 mesh points), one external to the nozzle (61×61 mesh points) and three blocks downstream of the nozzle exit (65×121, 97×121 and 97×121 mesh points). The mesh is very fine near the nozzle walls and near the jet axis in the plume, and becomes gradually coarser away from the axis. Grid-independence tests (see below) indicated this grid was adequate for the computations of the quantities examined in this work. Velocity, pressure and temperature boundary conditions consistent with experimental conditions are imposed at the upstream boundary inside the nozzle and a modest free-stream flow of $M = 0.05$ is imposed through a one-dimensional characteristic far-field boundary condition at all non-wall boundaries except the downstream boundary, where a subsonic outflow boundary condition is imposed. No-slip boundary conditions are imposed at all walls and axisymmetry is assumed.

The turbulence models employed in this investigation include both $k-\varepsilon$ and algebraic-stress two-equation models. The Reynolds stress, τ_{ij}, is modeled by the expression

$$\overline{\rho}\tau_{ij} = \frac{2}{3}\overline{\rho}k\delta_{ij} - 2\overline{\rho}C_{\mu}^{*}f_{\mu}\frac{k^2}{\varepsilon_s}[(S_{ij} - \frac{1}{3}S_{kk}\delta_{ij}) + \alpha_4\frac{k}{\varepsilon_s}(S_{ik}W_{kj} + S_{jk}W_{ki})$$

$$- \quad \alpha_5 \frac{k}{\varepsilon_s}(S_{ik}S_{kj} - \frac{1}{3}S_{kl}S_{kl}\delta_{ij})], \tag{1}$$

$S_{ij} = (1/2)(\tilde{u}_{i,j}+\tilde{u}_{j,i})$ and $W_{ij} = (1/2)(\tilde{u}_{i,j}-\tilde{u}_{j,i})$ being the symmetric and anti-symmetric parts of the mean-velocity-gradient tensor. Commas denote differentiation, the $\tilde{u}_i$ are velocity components and $\overline{\rho}$ is the average density. The remaining symbols are defined below.

The turbulent kinetic energy k and the solenoidal part of the dissipation rate ε_s (the total dissipation $\varepsilon = \varepsilon_s + \varepsilon_c$ is the sum of the solenoidal and curl-free dissipations; in the case of no compressibility correction $\varepsilon_c = 0$) are determined using the conservation equations

$$(\overline{\rho}k)_{,t} + (\overline{\rho}\tilde{u}_j k)_{,j} = -\overline{\rho}\tau_{mn}\tilde{u}_{m,n} - \overline{\rho}\varepsilon + \left((\mu + \overline{\rho}C_\mu^* f_\mu \frac{k^2}{\sigma_k \varepsilon_s})k_{,j}\right)_{,j}$$

$$(\overline{\rho}\varepsilon_s)_{,t} + (\overline{\rho}\tilde{u}_j \varepsilon_s)_{,j} = -\overline{\rho}C_{\varepsilon 1} f_1 \frac{\varepsilon_s}{k}\tau_{mn}\tilde{u}_{m,n} - \overline{\rho}C_{\varepsilon 2} f_2 \frac{\varepsilon_s \tilde{\varepsilon}}{k} + \left((\mu + \overline{\rho}C_\mu^* f_\mu \frac{k^2}{\sigma_\varepsilon \varepsilon_s})\varepsilon_{s,j}\right)_{,j} + \chi_w \tag{2}$$

For the $k-\varepsilon$ model, $\alpha_4 = 0$, $\alpha_5 = 0$ and $C_\mu^* = C_\mu = \text{const}$. In the k and ε_s equations, σ_k, σ_ε, $C_{\varepsilon 1}$ and $C_{\varepsilon 2}$ are constants and integration to the wall is possible using the damping functions f_μ, f_1 and f_2. Also in the ε equation, we have $\tilde{\varepsilon} = \varepsilon_s - \mu/\rho\,|\nabla\sqrt{k}|^2$ and χ_w, a wall-correction function.

The Gatski-Speziale algebraic-stress model [9] employs (1) with C_μ^*, α_4, and α_5 functions of k, ε and invariants of S_{ij} and W_{ij}. No wall damping of the Reynolds stress is required, so $f_\mu = 0$, and, in ISAAC, new f_1 and f_2 are introduced to preserve proper log-law behavior.

The Girimaji algebraic-stress model [10] also employs (1); in this case the coefficients C_μ^*, α_4 and α_5 are determined via the (explicit) solution of a cubic algebraic equation; see the work of Girimaji [10] for details of this solution and of the selection of the physically relevant root.

The models were tested both with and without the Sarkar compressibility correction [11], which gives for the compressible part of the turbulent dissipation ε_c the value $\alpha_c M_t^2 \varepsilon_s$, M_t being the turbulent Mach number $\sqrt{\tau_{ii}}/a_\infty$ and α being a constant taken here to be 0.5.

Results and Discussion

Computations were performed at jet total temperatures of 104^o F and 1550^o F. Extensive tests of the adequacy of the spatial resolution were conducted; comparison of runs with the full grid and with the grid coarsened by factors of 2 and 3 showed negligible differences. The value of y^+ for points adjacent to the walls of the nozzle was always less than 0.5 for the full-resolution computation,

indicating that the wall layers were satisfactorily resolved. All runs were continued well past the point where a steady state in the mean quantities had been reached.

Data for the 1550° F case appear in Figure 1. The mean velocity and temperature at the centerline are shown as computed using the various models discussed in the previous section and compared with experimental results [5]. While there is a good deal of variation in the computational results (this variation is much greater than the experimental uncertainty [5]), the ISAAC results are better, overall, than the PAB3D results. The centerline mean velocity for the 104° F case is shown (model by model) in Figures 2 and 3 and agreement is fairly good for both codes. While the results shown here are worse than one would like, they are better than earlier results [4].

The simulations employing the Sarkar compressibility correction were generally no better than those not. In the 104° F jet case, the correction makes the PAB3D predictions significantly worse, and the ISAAC predictions are slightly high by about as much as they were low for the computations without the compressibility correction. In the 1550° F jet case, the compressibility correction significantly improves the PAB3D results, but makes the ISAAC results dramatically worse.

Figure 1 shows a grouping of the results from each of the two codes; this grouping occurred in the other case as well. It suggests the differences in results may be due more to differences in the codes than to differences in the models. In order to further investigate these differences, the $k - \varepsilon$ model in PAB3D was implemented in ISAAC (except for the PAB3D form for χ_w, which involves derivatives not readily available in the ISAAC code), as was the PAB3D implementation of the Gatski-Speziale ASM. Comparisons between the ISAAC implementations of the models, the PAB3D implementations of the models and the PAB3D models implemented in ISAAC are shown in Figures 2 and 3 for the 104° F case. The results from ISAAC with its own models and with the PAB3D models were very similar for the $k - \varepsilon$ model and the Gatski-Speziale algebraic-stress model, indicating that the differences between the ISAAC and PAB3D results are primarily due to the codes themselves.

In summary, overall agreement of the computations with experiment is good. The two codes each gave fairly consistent results with the different turbulence models, and the differences between

the codes seemed to be greater than the differences between the models. Additional evidence for this was given by the computations with ISAAC using the PAB3D versions of the models, which gave results much closer to the ISAAC results with its own models than to the PAB3D results. Possible reasons for these differences between the results of the two codes include different handling of viscous fluxes (thin shear layer in PAB3D vs. full Navier-Stokes in ISAAC), first-order advection in the PAB3D turbulence equations vs. second-order advection in all equations in ISAAC and other differences in the numerical algorithms employed in the two codes.

Finally, we note that the aerodynamic input is only part of the story, and the MGB noise prediction may emphasize or de-emphasize different aspects of the input error.

Acknowledgements: The assistance of J. H. Morrison with ISAAC and P. Pao, J. Carlson and K. S. Abdol-Hamid with PAB3D is gratefully acknowledged. P. Pao and J. Carlson supplied the grid. The ISAAC and PAB3D CFD codes were made available by NASA Langley Research Center. This work was supported by NASA through the NASA Langley Research Center.

References

[1] Seiner, J. M., "A new rational approach to jet noise reduction," *Theoretical and Computational Fluid Dynamics*, Vol. 10, Nos. 1–4, 1998, pp. 373–383.

[2] Mani, R., *et. al.* , "High-velocity jet noise source location and reduction," Task 2, FAA-RD-76-79-II, 1977.

[3] Lighthill, M. J., "On sound generated aerodynamically. I. General theory," *Proceedings of the Royal Society of London*, Vol. A211, 1952, pp. 564-587.

[4] Barber, T. J., Chiapetta, L. M., DeBonis, J. R., *et al.*, "Assessment of parameters influencing the prediction of shear-layer mixing," *Journal of Propulsion and Power*, Vol. 15, No. 1, 1999, pp. 45–53.

[5] Seiner, J. M., Ponton, M. K., Jansen, B. J. and Lagen, N., "The effects of temperature on supersonic jet noise emission," DGLR/AIAA 14th Aeroacoustics Conference, Aachen, Germany, Paper No. 92-02-046, June 1992.

[6] Morrison, J. H., "A compressible Navier-Stokes solver with two-equation and Reynolds-stress turbulence closure models," NASA CR 4440, May 1992.

[7] Abdol-Hamid, K. S., "Implementation of algebraic-stress models in a general 3-d Navier-Stokes method (PAB3D)," NASA CR 4702, December 1995.

[8] Wilcox, D. C., *Turbulence Modeling for CFD*, DCW Industries, Inc., LaCanada, CA, 1993, Chapter 4.

[9] Gatski, T. B. and Speziale, C. G., "On explicit algebraic-stress models for complex turbulent flows," *Journal of Fluid Mechanics*, Vol. 254, September 1993, pp. 59–78.

[10] Girimaji, S. S., "Fully-explicit and self-consistent algebraic Reynolds-stress model," ICASE Report 95–82, Hampton, VA, December 1995.

[11] Sarkar, S., Erlebacher, G., Hussaini, M. Y. and Kreiss, H.O., "The analysis and modelling of dilatational terms in compressible turbulence," *Journal of Fluid Mechanics*, Vol. 227, June 1991, pp. 473–493.

List of Figures

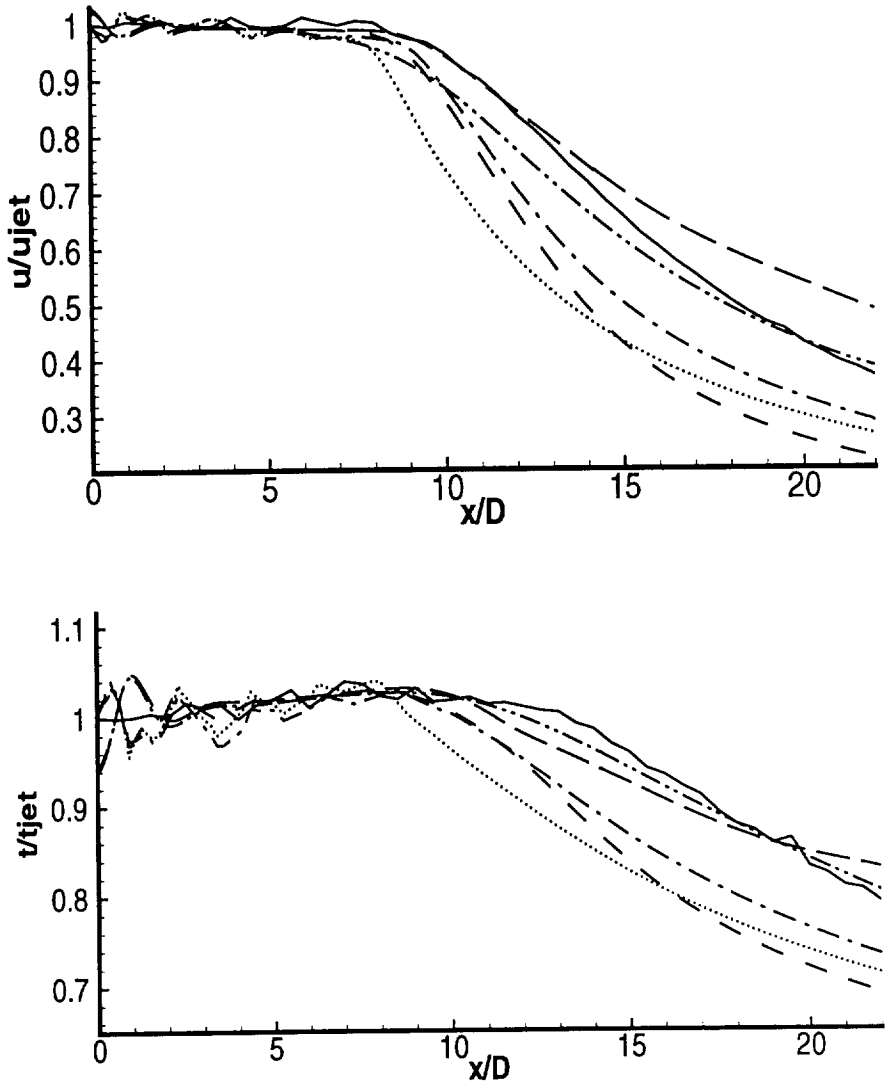

Figure 1: 1550° F case, no compressibility correction. Experiment, ——; ISAAC $k-\varepsilon$ model, $-\cdot\cdot$; ISAAC GS ASM, — —; PAB3D $k-\varepsilon$ model, $\cdots$; PAB3D GS ASM, $-\cdot$; PAB3D Girimaji ASM, – –.

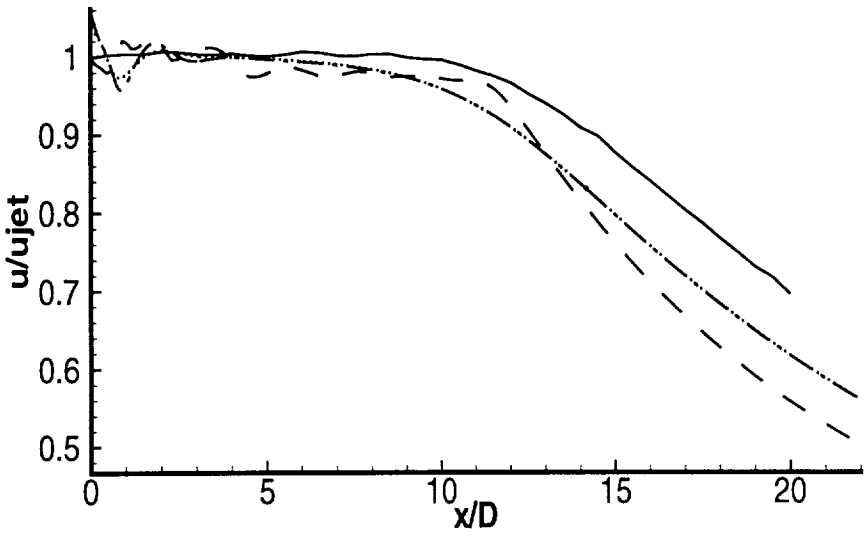

Figure 2: 104^o F case, comparison of k-ε models. Experiment, ——; ISAAC, – ·; PAB3D, – –; PAB3D model in ISAAC, · · ·.

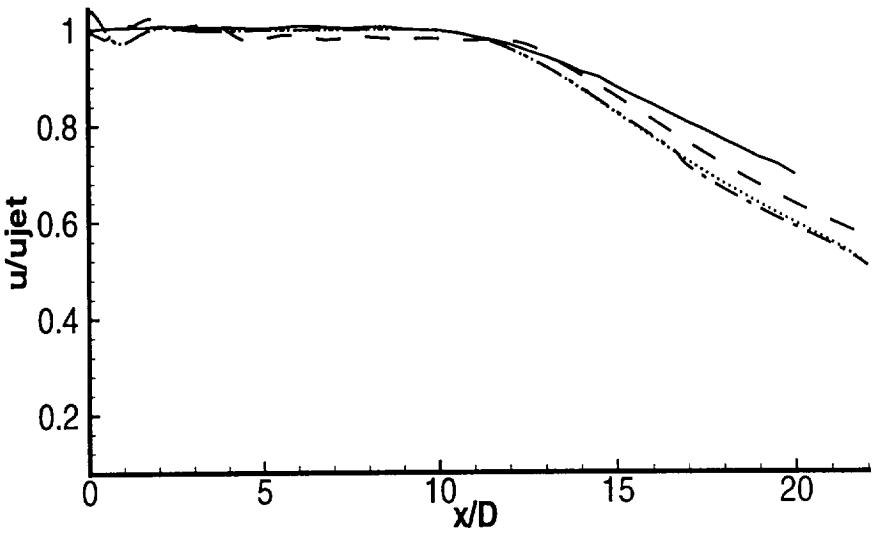

Figure 3: 104° F case, comparision of Gatski-Speziale ASMs. Experiment, ——; ISAAC, – ·; PAB3D, – –; PAB3D model in ISAAC, · · ·.

AIAA J. vol 38, p. 600, 2000

Grid-Size Dependence in the Large-Eddy Simulation of Kolmogorov Flow

S. L. Woodruff

Department of Mathematics and

Program in Computational Science and Engineering

Florida State University, Tallahassee FL 32306-4120

J. M. Seiner

National Center for Physical Acoustics

University of Mississippi

University, MS 38677

and

M. Y. Hussaini

Program in Computational Science and Engineering

Florida State University, Tallahassee FL 32306-4120

ABSTRACT

Through the use of both an *a priori* analysis of direct numerical simulation data and experiments with large-eddy simulations, a non-Smagorinsky grid-size dependence is established for the Smagorinsky sub-grid scale model for low numbers of resolved scales. It is shown that an increase in the Smagorinsky constant as the grid size is increased permits successful large-eddy simulations for cut offs approaching the energy-containing range of length scales. A detailed comparative analysis is made of the second-order turbulence quantities as determined by the differently resolutioned large-eddy simulations.

is periodic and shares many properties with common shear flows, but lacks many of the computational difficulties presented by homogeneous shear flow or such wall-bounded shear flows as channel flow or boundary-layer flow. Kolmogorov flow was originally proposed by Kolmogorov to his students as a simple flow for the study of stability problems in shear flows and has since been subjected to a number of stability analyses [5]. Turbulent Kolmogorov flow in two dimensions was studied by She [6]; three-dimensional direct numerical simulations of turbulent Kolmogorov flow employing the physical viscous stresses were performed by Shebalin and Woodruff [7]. Three-dimensional hyperviscosity simulations were performed by Borue and Orszag [8]. Some preliminary results from the present investigation have been presented earlier [9] and the present results have been recently presented [10].

The question of possible alternative grid-size dependences for the Smagorinsky model is here approached in two ways. First, an *a priori* analysis of a 64^3 direct-numerical simulation (DNS) data set is conducted. The fully-resolved velocity field from the DNS is filtered over a wide range of filter widths; for each filter width, both the Smagorinsky model formula and the Reynolds stress it is supposed to predict are evaluated. Comparing the two permits the filter width (or grid size) dependence of the Smagorinsky model to be assessed. The second approach to assessing the grid-size dependence of the Smagorinsky model is by LES experimentation: at each of a number of numerical resolutions, simulations are run with different values of the Smagorinsky constant. Determining which value of the Smagorinsky constant leads to the best results at a given resolution yields an empirically determined grid-size dependence.

Encouragingly, both approaches lead to similar conclusions about grid-size dependence. In both cases, an intermediate range of wave numbers (or grid sizes) was found where the standard Δ^2 grid-size dependence worked well. Beyond the low-wavenumber (coarse res-

olution) end of this range, an enhanced grid-size dependence is found to be necessary to give the best possible results, both in the *a priori* analysis of the DNS data set and for the LES experiments. Satisfactory LES results were achieved at suprisingly low resolutions when an appropriate grid-size dependence was used, though there was deterioration in the predictions, particularly of the turbulent shear stress.

The investigation outlined in this paper has sought to establish in a simple way that there is merit to the idea of altering the grid-size dependence of a sub-grid-scale model (in this case, the Smagorinsky model, with its traditional grid-size dependence based on inertial-range dynamics) in order to compensate for limited under-resolution in a large-eddy simulation. In keeping with this goal, a simple criterion for selecting the best Smagorinsky constant has been chosen (comparing the kinetic energies in different simulations) and simple criteria for assessing the adequacy of the under-resolved simulations (comparing several second-order statistical quantities) were employed in this preliminary investigation. More sophisticated approaches to fixing the Smagorinsky constant (including a theoretical discussion of its grid-size dependence as the energy-containing range is approached from above) and to assessing the usefulness of under-resolved large-eddy simulations are the subject of current investigation.

Following the problem statement and notational definitions of the next section, the *a priori* analysis of the DNS data set and the LES experiments are discussed. The paper concludes with a discussion of the results and their implication for the LES of complex flows.

Problem Statement and Numerical Considerations.

Kolmogorov flow is described by the Navier-Stokes equations subject to an artificial periodic body force with wavenumber k_f and amplitude $k_f v_o^2$. An appropriate nondimen-

sionalization consists of using $1/k_f$ for the reference length and $1/k_f v_o$ for the reference time; the Reynolds number is then $v_o/k_f\nu$. Taking the force vector to be in the positive x direction, the Navier-Stokes equations for an incompressible flow become

$$\frac{D\mathbf{v}}{Dt} = -\frac{1}{\rho}\nabla p + \frac{1}{Re}\nabla^2\mathbf{v} + \hat{\mathbf{i}}\,\sin z, \tag{1}$$

Periodic boundary conditions are imposed in all three directions, so the forcing wavenumber k_f reappears in the formulation in the ratio of the forcing wavenumber to the wavenumber of the longest wave contained in the box; this ratio will hereafter be denoted simply k_f.

The simulations examined in the present investigation have a Reynolds number of 28 and a forcing wavenumber of 6. This Reynolds number is sufficiently high to give fully developed turbulence (transition to turbulence occurs at $Re = 12 - 13$ in this nondimensionalization [6].) Previous experience with this flow [11] indicates the flow attains a statistically steady state more rapidly as the forcing wavenumber is increased; the use here of $k_f = 6$ provides fairly brief initial transients.

In the direct numerical simulation that provides the data set employed in the *a priori* analysis, the code of Shebalin [12] was used as configured for the earlier DNS found in Shebalin and Woodruff [7]. This code is pseudo-spectral with Fourier modes in the three spatial directions. A predictor-corrector time stepping algorithm is employed, with the viscous terms handled implicitly and the nonlinear terms handled explicitly.

The large-eddy simulations were performed with the same code, as adapted for LES for the simulations discussed in Woodruff, Shebalin and Hussaini [11]. The sub-grid-scale stresses τ_{ij} are incorporated as an explicit contribution to the time stepping; in this case the traditional Smagorinsky expression is used [13]

$$\tau_{ij} = -C_S\Delta^2\sqrt{S_{mn}S_{mn}}\;S_{ij}, \tag{2}$$

where C_S is the Smagorinsky constant, Δ^2 is a measure of the grid size and S_{ij} is the rate-of-strain tensor. As has been customary with LES using the Smagorinsky model and Fourier modes, the grid size (relative to the length of the sides of the box) is taken as $2\pi/N$, with N the number of modes in each coordinate direction. (All simulations considered here have the same number of modes in each coordinate direction.)

Since the fast-Fourier transform algorithm in the code expects the number of modes to be a power of two, runs with intermediate numbers of modes are performed by zeroing out the "excess" modes at each time step. For example, 24^3 runs are performed with the code set for 32^3 and with modes with wavenumbers of 13 through 16 zeroed out.

All DNS and LES runs reported here were initialized with a random initial velocity field with an exponential energy spectrum. Time series for the total kinetic energy, dissipation, etc. were used to establish that a statistically steady state had been reached.

A priori **Analysis.**

The goal of the *a priori* analysis is to determine what grid-size dependence gives the best fit between the sub-grid-scale turbulent stresses predicted by the Smagorinsky model and the true sub-grid-scale stresses when both are determined from a DNS data set. A 64^3 simulation was run as described in the previous section until a statistically steady state was reached, then the instantaneous velocity field from this simulation was used in the analysis.

The instantaneous velocity field was first filtered into super- and sub-grid components by means of a spectral cut-off filter (denoted $\langle\cdot\rangle$), which is to say that the velocity field was decomposed according to

$$u_i = \langle u_i \rangle + u_i' \tag{3}$$

with $\langle u_i \rangle$ containing all Fourier modes with wavenumber less than the cut off k_c and $u_i' = u_i - \langle u_i \rangle$ containing all Fourier modes with wavenumber greater than k_c. This decomposition

:rformed for all integer values of k_c running from 32 (no filtering, with all modes
ıed in the super-grid velocity $\bar{u}_i$) down to 2 (nearly complete filtering, with only the
ıd $k = 1$ modes contained in the super-grid velocity and all the others contained in
b-grid velocity u'_i.)

each of the cut-off wavenumbers k_c, the Smagorinsky representation of the sub-grid-
:tresses was computed, as well as the true stresses it is supposed to predict. The two
s $A_{ij} = \sqrt{S_{mn}S_{mn}}\, S_{ij}$ and $\tau_{ij} = -\langle u'_i u'_j \rangle$ that result are, according to the Smagorinsky
(eqn. 2), supposed to be proportional, with proportionality factor $C_S\Delta^2$. An empirical
ɔf the proportionality factor may be determined by reducing these second-rank tensor
varying in x, y and z to single numbers and taking their ratio.

ch of the components of these two tensors is a function of x, y and z; in this work,
ınction is reduced to a single number by taking the L^2 norm. Such a norm seems
priate for this problem, given the statistical homogeneity of the flow in the x and y
ions. The flow is not statistically homogeneous in the z direction, but even there flow
es do not cluster in particular regions of the flow domain and a norm which weights
y all parts of the flow seems reasonable. A more specialized norm will probably be
:ary in order to get useful results when such an analysis is applied to, say, turbulent
lary-layer flow or turbulent channel flow.

summary, then, for each filter cut-off wavenumber the velocity field is decomposed
upergrid and subgrid parts, the true sub-grid-scale stress and the Smagorinsky sub-
tress are formed, the L^2 norms are taken of each of the six independent components
: tensors, and the ratios are taken. In the results presented here, these ratios have
further divided by Δ^2, so that the result of the calculation is a grid-size dependent
orinsky constant C_S.

does exist. However, at this early stage of this research program, this measure of agreement provides a simple and surprisingly effective means of comparison.

In addition to the 32^3 reference simulations, large-eddy simulations were carried out at resolutions of 24^3, 16^3, 14^3 and 12^3. Time histories of results are shown in Figures 2 – 6; Table 1 contains parameters for the individual simulations and time averages of representative quantities over the statistically steady portion of the simulations' time histories. The time histories of the total kinetic energy for the most extreme case, the 12^3 simulations, are compared against the 32^3 reference simulations in Figure 2. Time histories are shown for simulations with values of the Smagorinsky constant that bracket the 32^3 reference plots; the two time histories are shown to give a rough impression of the sensitivity of the results to the change in C_S at each resolution. Thus, at least as far as the kinetic energy is concerned, adjustment of the Smagorinsky constant permits successful simulations for resolutions as low as 12^3. The extent to which other quantities are successfully simulated is examined in detail below.

Interpolated values for C_S were plotted in Figure 1 for comparison with the C_S values determined from the *a priori* analysis; it is seen that the LES experiments are consistent with the *a priori* results. The determination of similar variations in the Smagorinsky constant by these two independent means is strong evidence for the utility of alternative grid-size dependences in LES. Specifically, these results indicate that not only is the enhanced grid-size dependence necessary for low-resolutioned LES (as indicated by the *a priori* analysis), but it is sufficient (at least as far as the kinetic energy is concerned.)

Time histories of some other first and second order statistical quantities are shown in Figures 3 – 6. In each Figure, one simulation at each resolution is shown. (In all cases, the simulation is the one with the higher kinetic energy.) The statistical quantities are computed

using averages in the $x-y$ plane. Thus, $\bar{u}$ is a function of z; Figure 3 shows the L^2 norms of these functions. The fluctuating velocities $u' = u - \bar{u}$ and $w' = w - \bar{w}$ are represented by their L^2 norms in Figures 4 and 5. (Note these fluctuating velocities are different from the primed, fluctuating, velocities defined in the previous section.) The final plot, Figure 6, are of the L^2 norms of the correlation coefficient, defined by

$$C_{xz} = \frac{\overline{u'w'}}{\sqrt{\overline{u'^2}\ \overline{w'^2}}}. \tag{4}$$

Considering first the mean and fluctuating velocities of Figures 3–5, it is clear that almost all the simulations' predictions for these quantities cluster together quite well, once the initial transients have evolved into the statistical steady state. The exception is the 12^3 simulation, where it is clear that the limits of resolution have been exceeded. It is interesting to note that the 12^3 simulation has achieved the correct total kinetic energy by significantly overestimating the plane-averaged mean velocity and underestimating the fluctuating velocities, indicating the low resolution is suppressing the fluctuations.

The time series of the L^2 norm of the correlation coefficient shown in Figure 6 provide a more rigorous measure of the faithfulness of the simulations to the true turbulence physics, and their examination reveals weaknesses in the lower-resolutioned simulations. The C_{xy} and C_{yz} correlations (not shown) are reproduced fairly well by all simulations (even the 12^3 simulation); it is, however, the C_{xz} correlation, describing the Reynolds stress component that effects energy transfer from the mean to the fluctuating motion, where real breakdowns in the low-resolution simulations may be seen. Figure 6 shows that only the 24^3 simulation reproduces the steady-state value of C_{xz} correctly, with the 16^3 and 14^3 simulations giving values around half the true value. Curiously, and probably fortuitously, the 12^3 simulation does better here than the 14^3 and 16^3 simulations. It is worth noting as well (see Table 1) that the correlation coefficients are essentially unaffected by the changes in the Smagorinsky

constant at a given resolution.

Summary.

These results indicate that the low-resolution simulations not only correctly reproduce the total kinetic energy, but, except for the lowest-resolution, 12^3 simulation, correctly reproduce most of the other statistical quantities examined as well. The major failure of the low-resolution simulations was in the determination of the correlation coefficient C_{xz}, where only the 24^3 simulation came close to the correct value.

In addition to this failure of the low-resolution LES results in the prediction of the C_{xz} correlation, the results (as presented in Table 1) also show virtually no sensitivity of this correlation coefficient to changes in the value of the Smagorinsky constant. It may be concluded, then, that not only do the simulations performed with the Smagorinsky constant tuned to give the correct kinetic energy fail to give the right C_{xz}, but that no simple tuning of the Smagorinsky constant will give good results for the correlation coefficient. A more drastic adjustment of the model is necessary, and is being developed.

The breakdown of the under-resolved simulations at 12^3 and the failure of the under-resolved simulations to produce the correct correlation coefficient C_{xz} are likely related. Reducing the number of modes and the resolved scales inhibits the mechanism for the transfer of the energy from the mean to the fluctuating motion. At the 12^3 resolution, this inhibition has reached the point where insufficient energy flows into the fluctuating motion and so the mean energy is too high and the fluctuating energy is too low. Since, in this flow, as in other parallel flows, the energy transfer between the mean and fluctuating motion is mediated by the C_{xz} correlation, the inhibited energy transfer is reflected in incorrect values for that correlation.

The *a priori* results and the LES experiments described here indicate that, when used

with care, low-resolution simulations with an alternative grid-size dependence can give satisfactory results. Significant advances in the application of LES to complex turbulent flows of practical interest may thus be possible, provided reliable, general-purpose models are developed incorporating the concept of alternative grid-size dependences. Research into such models is currently under way.

Acknowledgement.

This work was supported by NASA through the NASA Langley Research Center.

References

[1] Gatski, T. B., Hussaini, M. Y. and Lumley, J. L., *Simulation and modeling of turbulent flows*, Oxford University Press, New York, 1996.

[2] Hussaini, M. Y., "On Large-Eddy Simulation of Compressible Flows," AIAA Paper 98-2802, June 1998.

[3] Speziale, C. G., "Turbulence Modeling for Time-Dependent RANS and VLES: A Review," *AIAA J.*, Vol. 36, 1998, pp. 173-184.

[4] Woodruff, S. L., Speziale, C. G., Hussaini, M. Y. and Erlebacher, G., "Continuous modeling for isotropic turbulence," preprint, 1998.

[5] See, for example, Théss, A., "Instabilities in two-dimensional spatially-periodic flows. Part I : Kolmogorov flow," *Phys. Fluids A*, Vol. 4, 1992, p. 1718; Platt, N., Sirovich, L. and Fitzmaurice, N., "An investigation of chaotic turbulent flow," *Phys. Fluids A* Vol. 3, 1991, p. 681.

[6] She, Z. S., "Meta-stability and vortex pairing in the Kolmogorov flow," *Phys. Lett. A*, Vol. 124, 1987, p. 161; She, Z. S., "Large-scale dynamics and transition to turbulence," *Current Trends in Turbulence Research*, AIAA, Washington, D. C., 1988, p. 374

[7] Shebalin, J. V. and Woodruff, S. L., "Kolmogorov flow in three dimensions," *Phys. Fluids*, Vol. 9, 1997, p. 164.

[8] Borue, V. and Orszag, S. A., "Numerical study of three-dimensional Kolmogorov flow at high Reynolds numbers," *J. Fluid Mech.*, Vol. 306, 1996, p. 293.

[9] Woodruff, S. L., Seiner, J. M. and Hussaini, M. Y., "Grid-size-dependence considerations for sub-grid-scale models for LES of Kolmogorov flow," American Physical Society Division of Fluid Dynamics meeting, San Francisco, Nov. 1997.

[10] Woodruff, S. L., Seiner, J. M. and Hussaini, M. Y., "Grid-size Dependence in the Large-Eddy Simulation of Kolmogorov Flow," AIAA Paper 99-3777, June 1999.

[11] Woodruff, S. L., Shebalin, J. V. and Hussaini, M. Y., "Large-eddy simulations of non-equilibrium turbulent Kolmogorov flows", ICASE Report.

[12] Shebalin, J. V., "Broken symmetry in ideal magnetohydrodynamic turbulence," *Physics of Plasmas*, Vol. 1, 1994, pp. 541–7.

[13] Smagorinsky, J., "General circulation experiments with the primitive equations, part I: The basic experiment," *Mon. Wea. Rev.,* Vol. 91, 1963, p. 99.

Table 1: Simulation parameters and temporal averages of results.

No. Modes	C_S	K	$\|\|\bar{u}\|\|$	$\|\|u'\|\|$	$\|\|v'\|\|$	$\|\|w'\|\|$	C_{zx}
32	0.006	2.33	0.93	1.24	0.89	1.21	0.41
32	0.008	2.08	0.74	1.20	0.82	1.22	0.44
24	0.0045	2.48	0.88	1.36	0.96	1.19	0.40
24	0.0056	2.33	0.85	1.32	0.90	1.17	0.41
16	0.008	2.49	0.96	1.28	0.88	1.28	0.25
16	0.012	2.26	1.04	1.21	0.71	1.20	0.27
14	0.0077	2.38	0.85	1.26	0.82	1.33	0.27
14	0.010	2.18	0.82	1.15	0.69	1.37	0.28
12	0.0087	2.44	1.75	0.97	0.81	0.45	0.32
12	0.0096	2.25	1.69	0.92	0.78	0.42	0.34

List of Figures

Figure 1: Smagorinsky constant C_S as function of grid-size, as determined by *a priori* analysis (solid line) and LES experiments (dots).

Figure 2: Kinetic energy versus time for 32^3 simulation with $C_S = 0.006$ (solid line), 32^3 simulation with $C_S = 0.008$ (long-dashes), 12^3 simulation with $C_S = 0.0087$ (dashed line), 12^3 simulation with $C_S = 0.0096$ (dotted line).

Figure 3: $\|\bar{u}\|$ versus time for 32^3 simulation with $C_S = 0.006$ (solid line), 24^3 simulation with $C_S = 0.0045$ (long dashes), 16^3 simulation with $C_S = 0.008$ (dashed line), 14^3 simulation with $C_S = 0.010$ (dash-dotted line), 12^3 simulation with $C_S = 0.0087$ (dotted line).

Figure 4: $\|u'\|$ versus time for 32^3 simulation with $C_S = 0.006$ (solid line), 24^3 simulation with $C_S = 0.0045$ (long dashes), 16^3 simulation with $C_S = 0.008$ (dashed line), 14^3 simulation with $C_S = 0.010$ (dash-dotted line), 12^3 simulation with $C_S = 0.0087$ (dotted line).

Figure 5: $\|w'\|$ versus time for 32^3 simulation with $C_S = 0.006$ (solid line), 24^3 simulation with $C_S = 0.0045$ (long dashes), 16^3 simulation with $C_S = 0.008$ (dashed line), 14^3 simulation with $C_S = 0.010$ (dash-dotted line), 12^3 simulation with $C_S = 0.0087$ (dotted line).

Figure 6: $\|C_{xz}\|$ versus time for 32^3 simulation with $C_S = 0.006$ (solid line), 24^3 simulation with $C_S = 0.0045$ (long dashes), 16^3 simulation with $C_S = 0.008$ (dashed line), 14^3 simulation with $C_S = 0.010$ (dash-dotted line), 12^3 simulation with $C_S = 0.0087$ (dotted line).

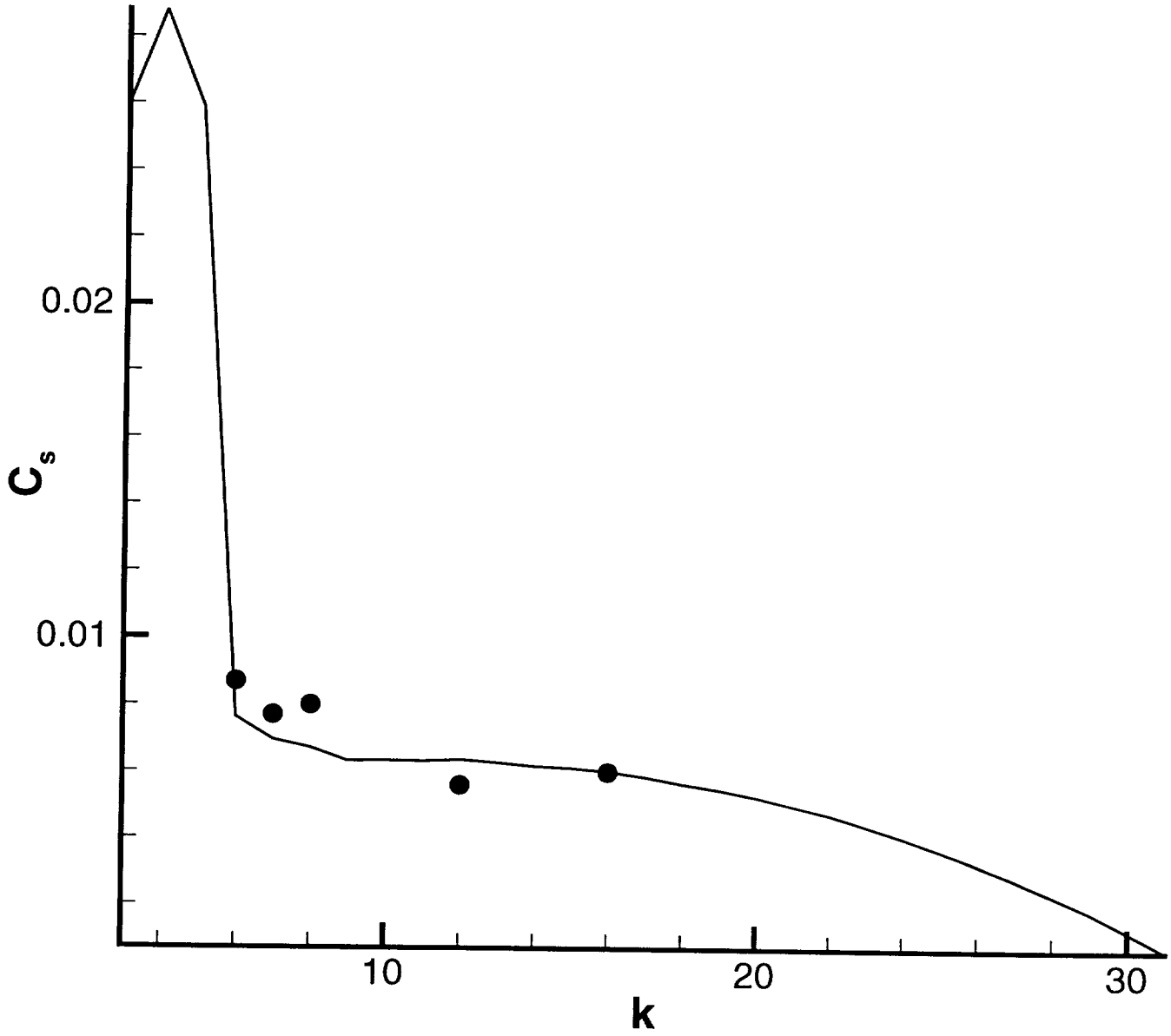

Figure 1: Smagorinsky constant C_S as function of grid-size, as determined by *a priori* analysis (solid line) and LES experiments (dots).

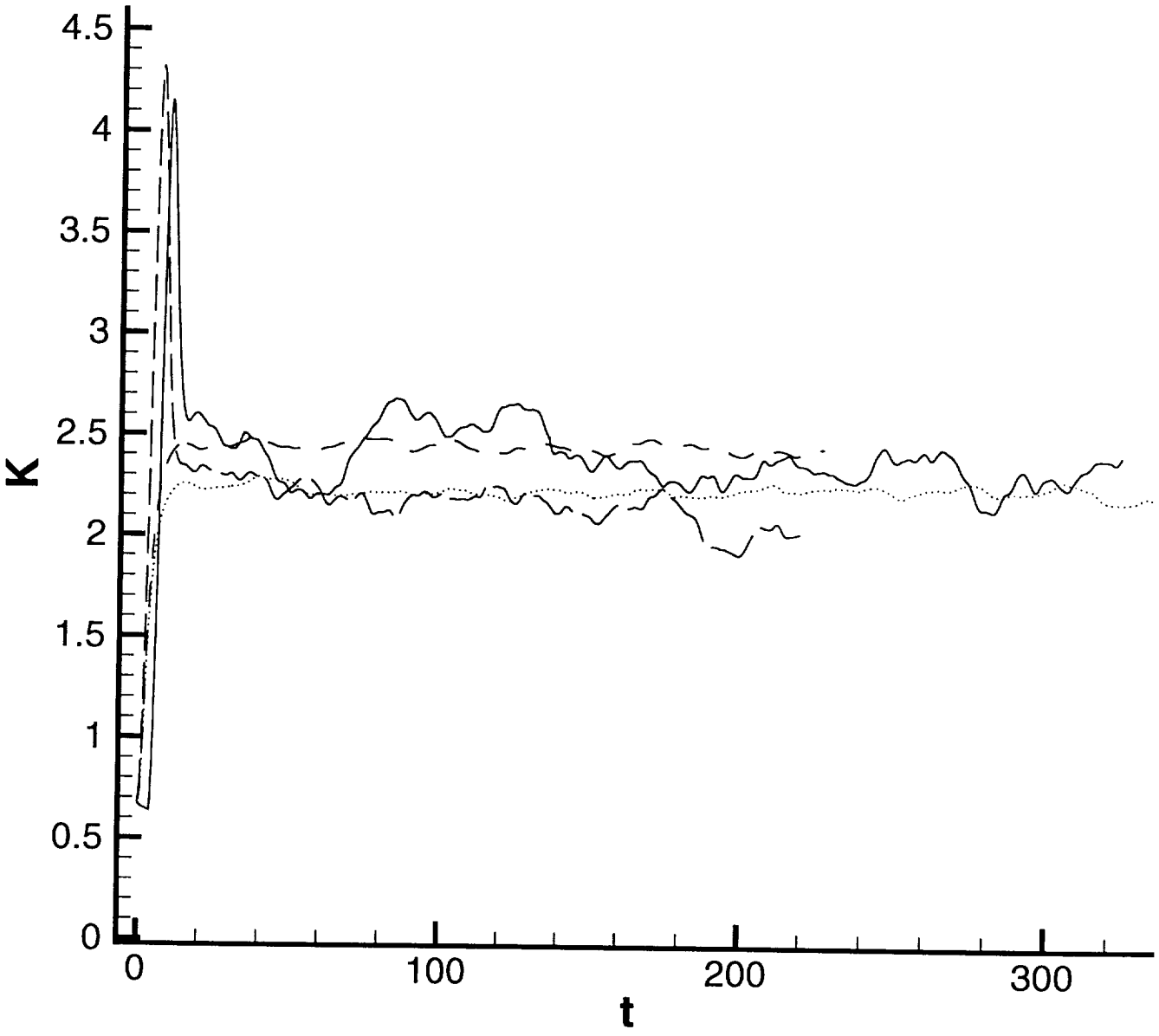

Figure 2: Kinetic energy versus time for 32^3 simulation with $C_S = 0.006$ (solid line), 32^3 simulation with $C_S = 0.008$ (long-dashes), 12^3 simulation with $C_S = 0.0087$ (dashed line), 12^3 simulation with $C_S = 0.0096$ (dotted line).

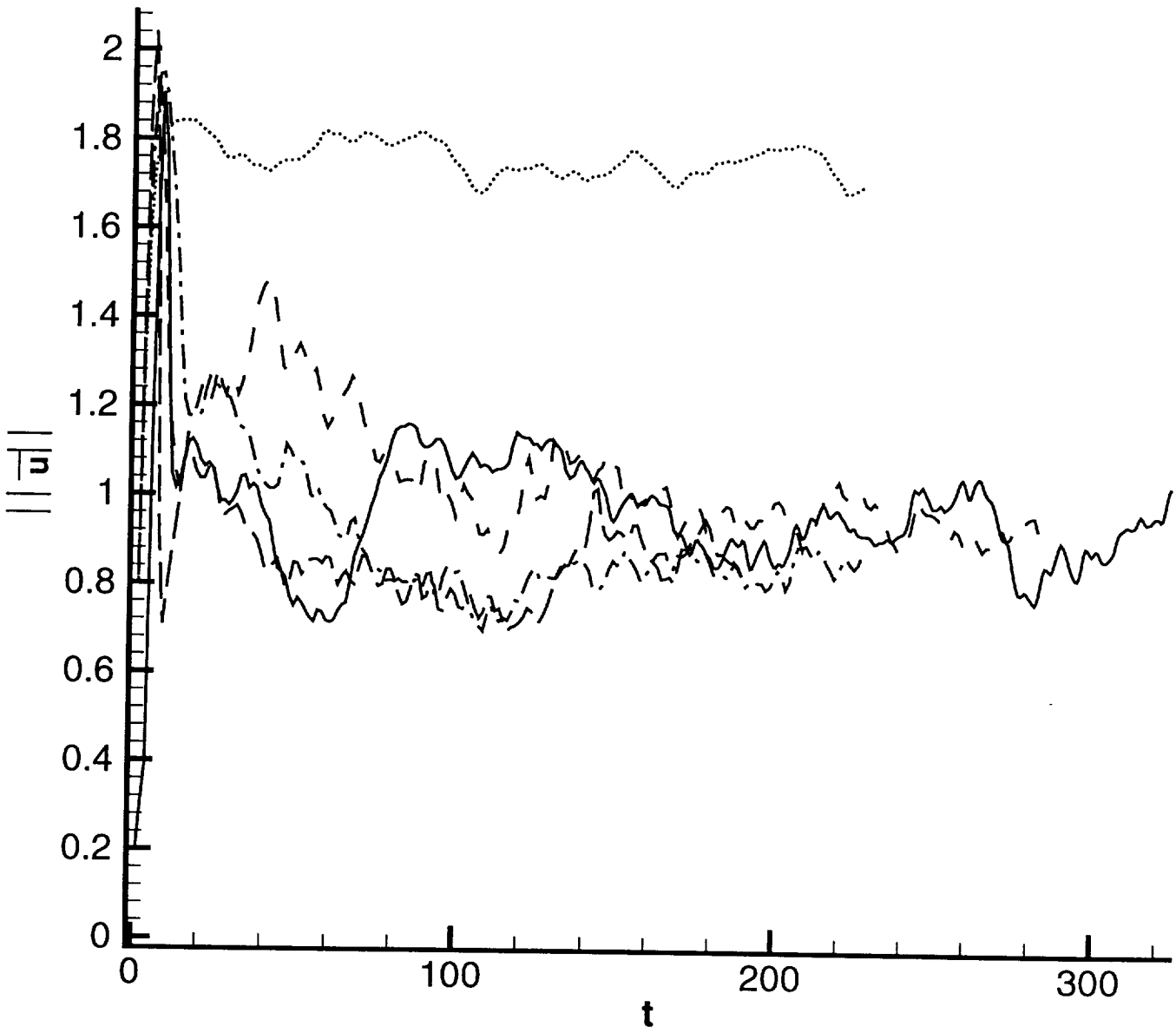

Figure 3: $\|\bar{u}\|$ versus time for 32^3 simulation with $C_S = 0.006$ (solid line), 24^3 simulation with $C_S = 0.0045$ (long dashes), 16^3 simulation with $C_S = 0.008$ (dashed line), 14^3 simulation with $C_S = 0.010$ (dash-dotted line), 12^3 simulation with $C_S = 0.0087$ (dotted line).

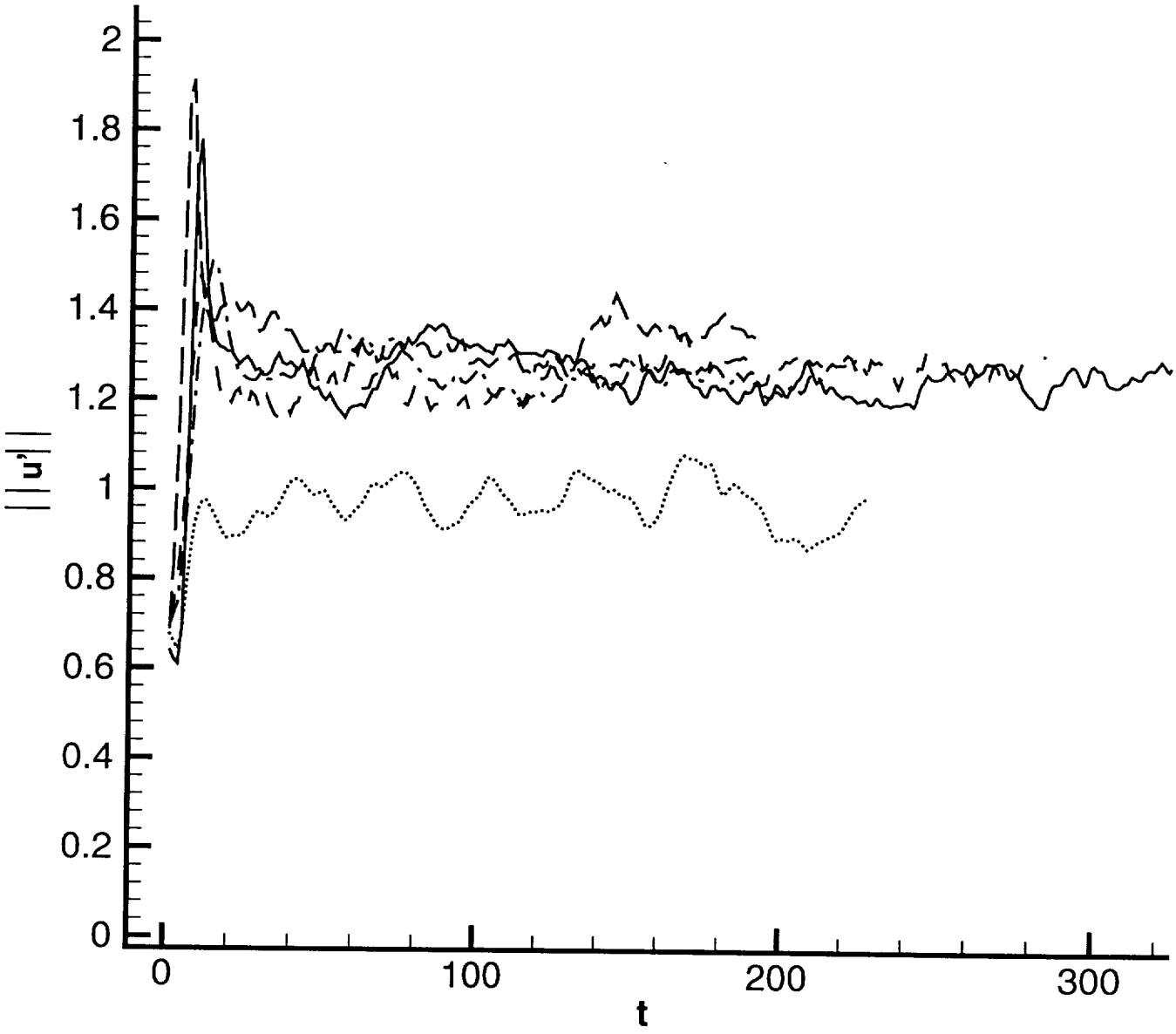

Figure 4: $\|u'\|$ versus time for 32^3 simulation with $C_S = 0.006$ (solid line), 24^3 simulation with $C_S = 0.0045$ (long dashes), 16^3 simulation with $C_S = 0.008$ (dashed line), 14^3 simulation with $C_S = 0.010$ (dash-dotted line), 12^3 simulation with $C_S = 0.0087$ (dotted line).

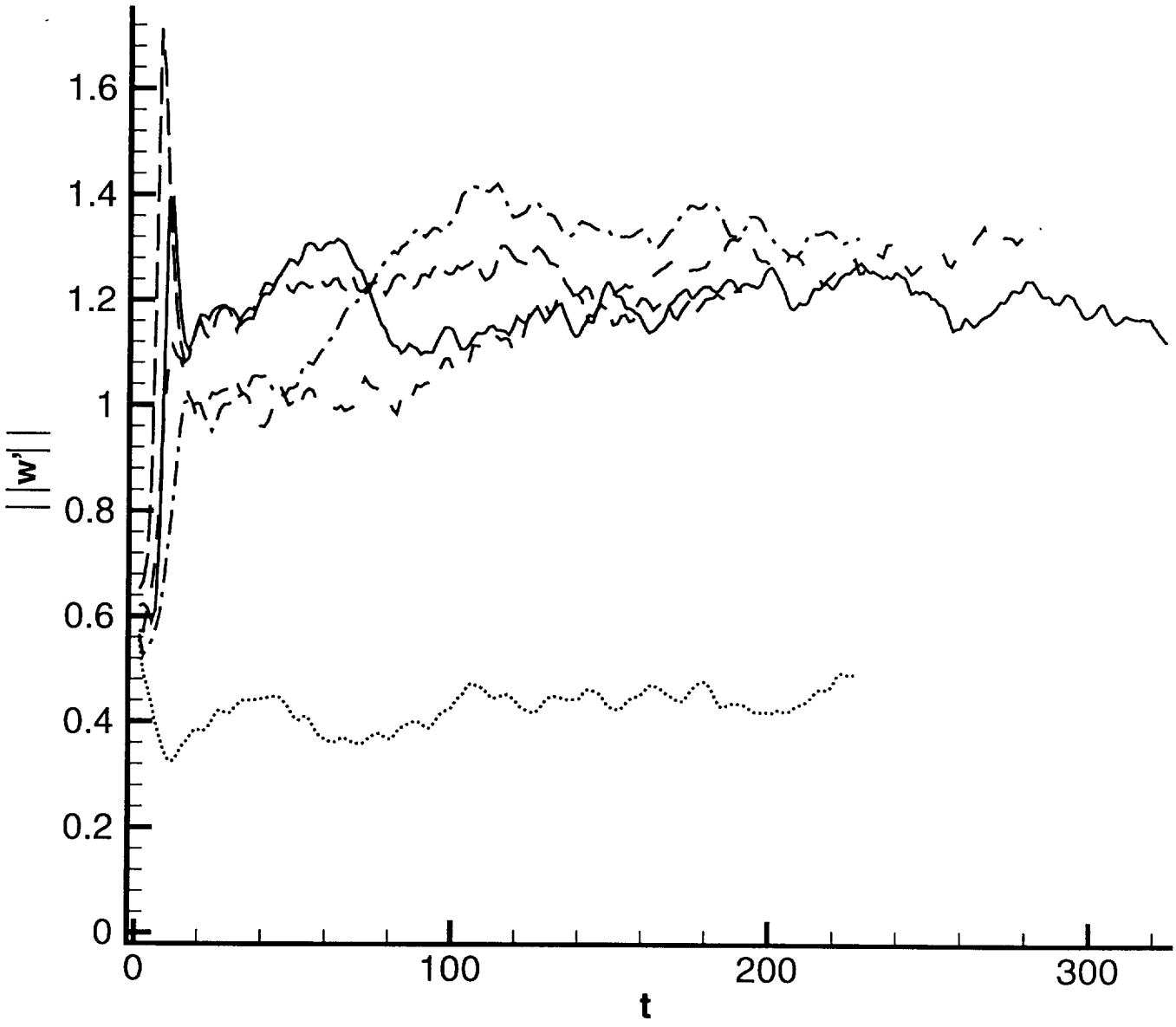

Figure 5: $\|w'\|$ versus time for 32^3 simulation with $C_S = 0.006$ (solid line), 24^3 simulation with $C_S = 0.0045$ (long dashes), 16^3 simulation with $C_S = 0.008$ (dashed line), 14^3 simulation with $C_S = 0.010$ (dash-dotted line), 12^3 simulation with $C_S = 0.0087$ (dotted line).

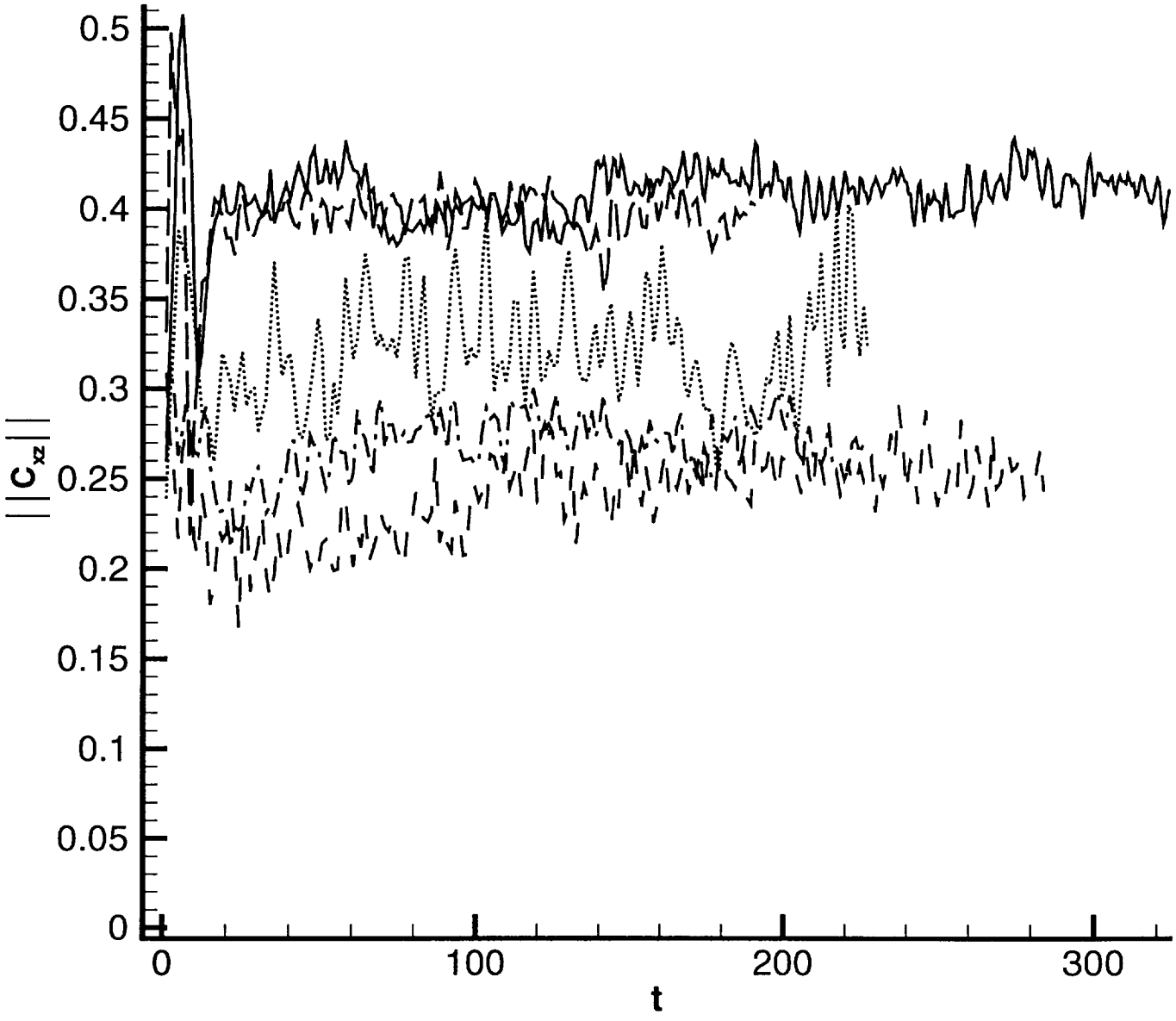

Figure 6: $\|C_{xz}\|$ versus time for 32^3 simulation with $C_S = 0.006$ (solid line), 24^3 simulation with $C_S = 0.0045$ (long dashes), 16^3 simulation with $C_S = 0.008$ (dashed line), 14^3 simulation with $C_S = 0.010$ (dash-dotted line), 12^3 simulation with $C_S = 0.0087$ (dotted line).